The Seventh International Colloquium on Bluff Body Aerodynamics and Applications (BBAA7)
Shanghai, China; September 2-6, 2012

Numerical Simulation with PCA analysis of flow around 1:5 rectangular cylinder

Shining Zhang[a], Zhiwen Zhu[a]

([a]*Center of Wind Engineering, Hunan University, Changsha, China*)

ABSTRACT: The unsteady flow field around a two-dimensional rectangular prism with aspect ratio of 5 is studied by using Unsteady Reynolds-Averaged Navier-Stokes (URNS) equations. Fundamental flow characteristics are provided with numerical simulation and compared with the experiment, satisfactory agreement is obtained consequently. The aim of this paper is to find the nature of the fluctuating pressure on the surface of the rectangular cylinder indicated by the Principal Component Analysis. To better understand the vortex shedding phenomenon, flow visualization is provided. At last, effects of Reynolds number ranged from 1.03×10^4 to 1.03×10^6 on the flow characteristics are discussed.

KEYWORDS: Rectangular cylinder, CFD, PCA, vortex shedding, Reynolds number effects.

1 INTRODUCTION

In bridge engineering, rectangular shape are commonly employed as the cross section of bridge components, such as the plate girder, tower, pier, etc. The infamous bridge destroyed by the wind-induced vibration and shocking the civil engineers is old Tacoma Narrows Crossing, with its H-shaped stiffening girder at chord-to-thickness ratio very close to 5. Therefore investigation of the flow past such kind of cross section is of great concern. As a benchmark problem, rectangular cylinder had been studied by many researchers over the years through wind tunnel test, numerical simulation method and site measurement.

The aerodynamics of a rectangular cylinder with the aspect ratio of 5 as a benchmark problem has been studied for many years. Both the two-dimensional (2-D) and three-dimensional (3-D) features of the flow characteristics around rectangular cylinders have been clarified in several studies, e.g. in Claudio Mannini(2010), Luca Bruno(2009), Gunter Schewe(2009). Most of what they explored was the mean pressure coefficient distributions, nevertheless, usually it is the fluctuating pressure that mainly affects the variation of aerodynamic forces, therefore fluctuating pressure should be well considered and analyzed when dealing with aerodynamics.

This paper deals with the two-dimensional (2-D) numerical simulation of flow past a rectangular cylinder with a chord-to-thickness ratio B/D=5 at zero flow incidence. The reattachment which significantly relates to the pressure recovery is calculated, some other natures of flow characteristics is analyzed, mainly including principal component of pressure distribution around the upper surface and periodic vortex shedding. The Principal Component Analysis which is recognized an effective method to represent the unsteady flow is employed to deal with the fluctuating pressure. Finally, the effects of Reynolds number on those flow characteristics have been investigated. Through those flow characteristics, we can better understand the fluctuation of aerodynamic forces and find the main factors leading to those variations.

Although the resulting flow field is known to be three dimensional, the current two-dimensional calculation is able to predict important flow properties (D. K. Tafti and S. P. Vanka,

1991). The current 2-D numerical simulation is adopted to explore its capacity and advantages through comparison with the experimental results and three-dimensional (3-D) calculations. Also, this paper will definitely lay a foundation for 3-D research and the results analyzed from 2-D are used to compare with latter 3-D study in order to find the indispensable role and improvement of 3-D effects.

2 FLOW MODEL AND PCA THEORY

2.1 Governing equation and turbulent model

The unsteady, incompressible, 2D viscous fluid flow around the rectangular cylinder is modeled by means of the time-averaged Navier-Stokes equations as follows:

$$\frac{\partial \overline{u_i}}{\partial x_i} = 0 \tag{1}$$

$$\frac{\partial}{\partial t}\left(\rho \overline{u_i}\right) + \frac{\partial}{\partial x_j}\left(\rho \overline{u_i}\,\overline{u_j}\right) = -\frac{\partial \overline{p}}{\partial x_i} + \frac{\partial}{\partial x_j}\left(\mu \frac{\partial \overline{u_i}}{\partial x_j} - \rho \overline{u_i' u_j'}\right) \tag{2}$$

Where x and t are the space and time coordinates, $\overline{u}$ and $\overline{p}$ are the time-averaged velocity and pressure, μ is the turbulent viscosity and ρ is the fluid density. $\rho u_i' u_j'$ is the Reynolds stress.

The Boussinesq hypothesis to relate the Reynolds stresses to the mean velocity gradients:

$$-\rho \overline{u_i' u_j'} = \mu_t \left(\frac{\partial \overline{u_i}}{\partial x_j} + \frac{\partial \overline{u_j}}{\partial x_i}\right) - \frac{2}{3}\left(\rho k + \frac{\partial \overline{u_i}}{\partial x_i}\right)\delta_{ij} \tag{3}$$

In consideration of complex flow near the wall of rectangular cylinder, the shear-stress transport (SST) $k-\omega$ model is employed in present simulation, since $k-\omega$ model effectively blend the robust and accurate formulation of the $k-\varepsilon$ model in the near-wall region with the free-stream independence of the $k-\varepsilon$ model in the far field.

2.2 Principal Component Analysis (PCA) theory

In the study of the pressure fluctuation around bluff bodies using PCA, Holmes(1990) pointed out that the covariance matrix of the pressure fluctuation contains information on the magnitude and distribution of the underlying fundamental modes of the pressure distribution around a body. Studies show that these modes are represented by the eigenvectors of the corresponding covariance matrix of the pressure distribution on the body's surface.

Mathematically, to perform PCA on a data set x, the eigenvalues, λ_i and the eigenvector, e_i of a covariance matrix C_x can be evaluated from the solution of :

$$C_x e_i = \lambda_i e_i \tag{4}$$

The eigenvalues is calculated as the roots of ,

$$\left|C_x - \lambda_i I\right| = 0 \tag{5}$$

Where $i = 1,2,\ldots,n$, n is the total number of the input data and I is the identity matrix.

The eigenvalues are associated with the variance of each of the components. Each eigenvalue is accompanied by an eigenvector, the nonzero vector e_i that satisfies Eq. 4.

The principal components of PCA are made up of columns of eigenvectors of the covariance matrix C_x. By arranging the eigenvectors in the order of descending eigenvalue($\lambda_i > \lambda_{i+1...}$), one gets the most significant changes of the variables in the data in the first principal component.

In PCA, the variables x are decomposed in the process of the eigenanalysis. It is possible to regenerate the variables x using the PCA results as follows:

$$x = A^T Y + \mu_x \tag{6}$$

Where A^T is the transpose matrix whose columns are given by the eigenvector of the covariance matrix and Y is the coefficients of the principal components. μ_x is the mean value of the data set x.

From Eq. 6, the original data can be reconstructed from the terms on the right hand side of the equation to see how well the original data can be represented from the few principal components in the analysis.

3 COMPUTATIONAL MESHES

As we all know that the quality of the computation mesh plays a crucial role in the reliability of numerical simulation. For this reason, a simple grid-convergence study is outlined in order to choose a reasonable grid for the following computations. In this paper the stationary rectangular cylinder at zero-degree angle of attack ($\alpha = 0^\circ$) and Reynolds number Re=$U_\infty B / \nu = 3.42 \times 10^5$ (B is the width of the cylinder and ν the air kinematic viscosity) is chosen as test case.

Three 2-D hybrid grids were investigated, whose main characteristics are listed in Table 1. The fine grid is display in Fig.1 (left). In order to guarantee the accuracy of numerical simulation, the grid along the surface is generated by structured grid. Additionally, the only difference among those three grids is the level of grid refinement in structured grid zone close to the body surface.

The Dirichlet condition on the velocity field and sub-grid kinetic energy is imposed on the inlet boundary. Neumann conditions on the normal component of the stress tensor $\boldsymbol{T}$, as well as the same Dirichlet conditions on turbulence kinetic energy k, are imposed at the outlet boundary. Symmetry conditions are imposed on the both upper and lower boundary of the computational domain, while the no-slip boundary condition is imposed on the body surface, as indicated in Fig.1 (right). In order to represent the imposed physical boundary and reduce the influence from outside boundary, the distance between outside boundaries of the computational domain and the center of the body has also been meticulously selected, as shown in Fig.1 (right).

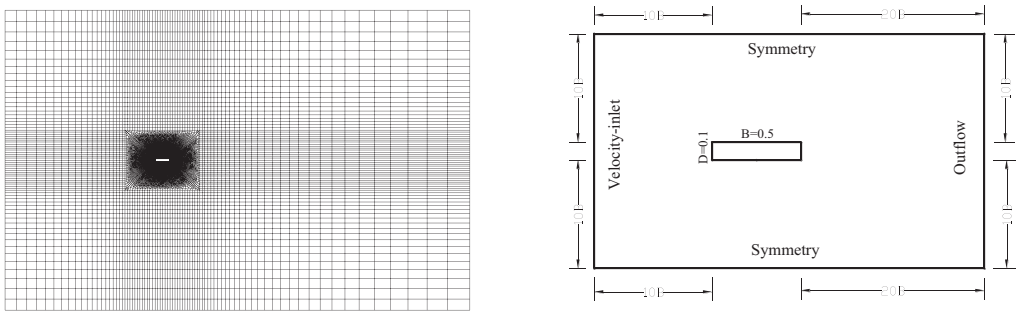

Fig.1. Fine grid and whole computational zone.(units: m)

Table 1. Main properties of grid system. The parameter δ and $\Delta y_{j+1} / \Delta y_j$ is the height and stretching factor of the first structured layer closest to the body surface respectively.

Grid	δ / B	$\Delta y_{j+1} / \Delta y_j$	Total cells	Structured cells	Unstructured cells	Good mesh
Coarse	2.5E-6	1.1	60,883	38,300	22,583	91.7%
Fine	6.0E-6	1.1	94,483	71,900	22,583	89.3%
Finest	6.0E-6	1.03	139,283	116,335	22,948	88.0%

Table 2. Present results of different grid arrangement in comparison with other literature (α =0°)

Grid	Reynolds number	max y^+	St	C_D	$C_L^{'}$	$C_D^{'}$
Coarse	3.42×10^5	4	0.114	1.05	0.1	0.006
Fine	3.42×10^5	0.1	0.113	1.09	0.16	0.009
Finest	3.42×10^5	0.1	0.116	1.08	0.1	0.004
Experiments(Schewe,2009)	2.64×10^5	-	0.111	1.029	0.4	-
Okajima(1983) I=0.4%	0.42×10^5	-	0.110	-	0.15	-
K. Snimada and T. Ishihara ($k-\varepsilon$ model)	-	-	0.118	1.0	0.05	-

After a series of trial calculation with several time-step size (dt), dt=0.0005s is eventually verified small enough, even conservative to resolve the dominant unsteady flow phenomena. Table 2 shows the computed St, the mean drag coefficient C_D and the standard deviation of lift and drag coefficients, $C_L^{'}$ and $C_D^{'}$. The table also reports the maximum value of the maximum value of the computed first-layer non-dimensional distance from the wall, defined as Yplus, y^+, which is recommended around 1 for the higher Reynolds number when utilizing the SST $k-\omega$ turbulent model. Considering the results obtained, the fine grid is found to be a reasonable compromise between accuracy and computational time cost. Therefore this grid will be employed in the following simulations.

4 FLOW RESULTS

4.1 Fundamental flow characteristics

Fig.2 displays the mean and standard-deviation values of the pressure coefficient on the body surface with several wind tunnel results reported for comparison. Usually, since the pressure fluctuation at some points (x/D=0 and 5) is thought to be sensitively affected by the approaching flow, those points have been excluded from the following discussion. The mean pressure coefficient C_P is defined as

$$C_P = (p - p_\infty) / 0.5\rho U^2 \tag{7}$$

Obviously, the mean C_P computed with 2-D SST $k-\omega$ model agrees well with the numerical simulation conducted by T. Ishihara (2001) and the experiment performed by Matsumoto (2005) at higher Reynolds number of 200,000, while a small discrepancy exists near leading edge at Re=100,000. The mean pressure coefficient distribution on the upper surface of rectangular cylinder exhibits a pressure increase toward the rear end. This is the inclination of reattachment of the flow which leads to pressure recovery toward the trailing edge, and this reattachment can be confirmed by streamlines in flow visualization. As for the standard deviation of the pressure coefficient, $C_P^{'}$, the wind tunnel data present a significant dispersion. This is probably due to the fact that the distribution of $C_P^{'}$ is more sensitive to the experimental boundary conditions than the mean values of pressures. Also, from the experiment results (Matsumoto,2005) we can con-

clude that $C_P^{'}$ is relevant to the Reynolds number to some extent. Although the present result of $C_P^{'}$ also distinct from the experiment, it predicts nearly the same position of the peak of $C_P^{'}$, which is a crucial parameter indicating the existence of vortex in this region. As a result, the experimental data provided the position at about x/D=3.7, while this present simulation give the location at x/D=3.85. From the mean friction coefficient distribution on the upper surface of the rectangular cylinder, the present calculation gives a value of x_R/B=0.903, which is slightly larger (3.2%) than the experiment estimated by Matsumoto et al. (2002) based on the distribution of the time-averaged pressure coefficient C_P and RMS value $C_P^{'}$ (x_R/B=7/8).

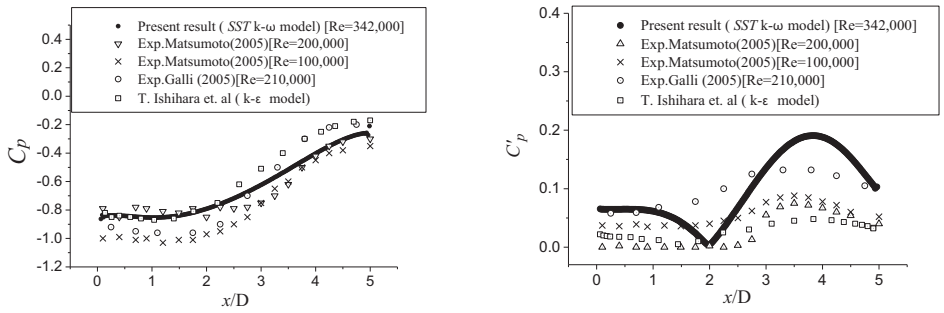

Fig.2. Comparison of pressure coefficient distribution with experiments (Matsumoto,2005 and Galli,2005), left: mean, right: standard deviation.

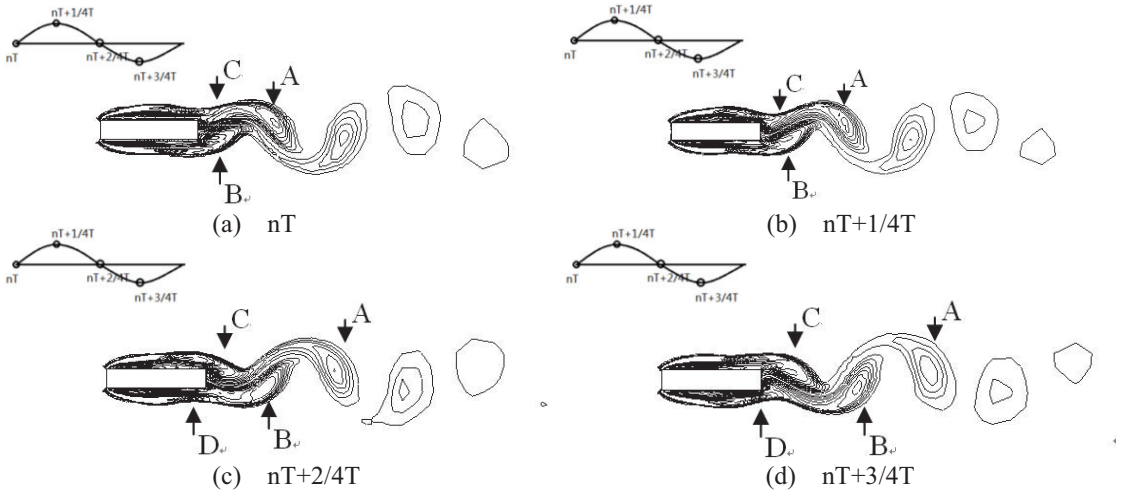

Fig.3. Snapshots of vorticity magnitude in flow field.

Fig.3 clearly describes the shedding of vortices from the rectangular cylinder. In (a), the total lift force on the bluff body is zero, and three vortices are labeled by A, B and C behind the cylinder. A is already shed, preparing to exit into the wake. B was originally from the lower side of the cylinder and is still attached to the rear side of the cylinder. In (b), A moves further towards the wake, while C moves to the center of the rear side surface. In (c), half a cycle of the lift force is completed, and it may be concluded that the vorticity close to the cylinder in (c) is similar to those in (a), but only reversed. In (c), B is completely shed off the rear side surface while a new vortex D is formed at the lower side behind the cylinder.

4.2 Principal Component Analysis results

In this section, the PCA theory is utilized to identify the fluctuating pressure. The analysis is carried out based on the procedures outlined in the previous section (section 2.2). As mentioned

above, the first principal component corresponds to the eigenvalues with the highest values, which quantifies the largest variation of pressure with respect to the total pressure changes in the flow within the time series considered in the analysis.

The principal components represent the fluctuating nature of the flow. Fig.4 depicts the first and second principal component of the pressure distribution on upper surface of the cylinder. It is found that the largest pressure fluctuation is appeared near the trailing edge of the section (upper surface). This indicates the presence of vortex structures at these regions and the peak of the first principal is located at x/D=3.85, which agrees well with the RMS values of C_P' distribution shown in Fig.2. Compared to the first principal component, the second one owns a more even pressure distribution (comparing total area on both sides of the *x*-axis in the graphs).

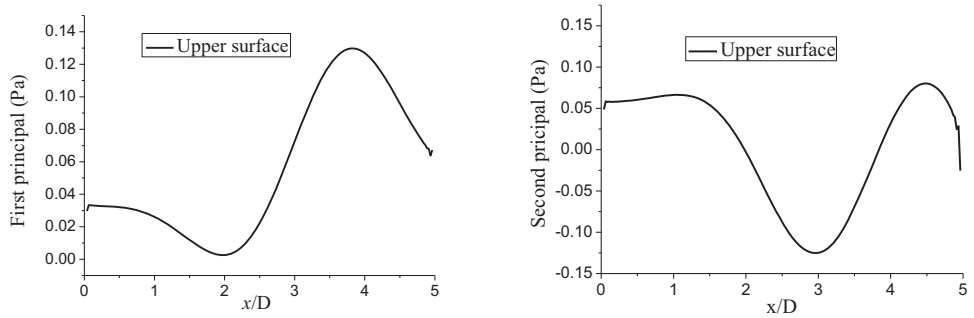

Fig.4. First and second principal component of pressure distribution on upper surface.

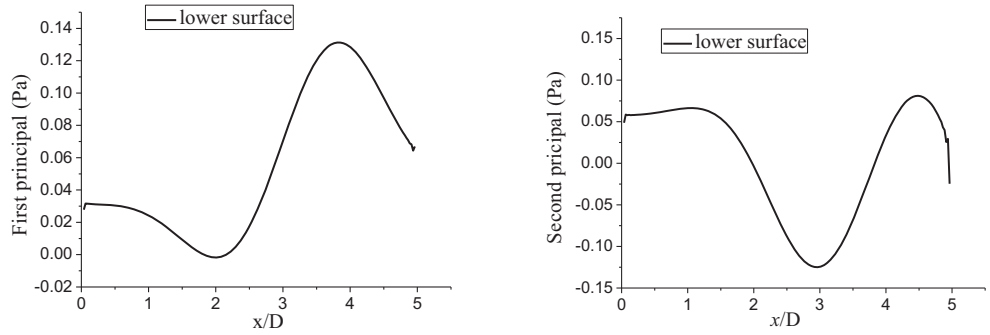

Fig.5. First and second principal component of pressure distribution on lower surface.

Fig.5 displays the first and second principal component of the pressure distribution around lower surface of the cylinder. Notice that the pressure distribution on the upper and lower surfaces of the cylinder shows different trends in the first principal component compared to the second principal component. A large amplitude pressure distribution appears near the trailing edge of the cylinder in the first principal component, while it happens at the middle part of the cylinder in the second principal component (Fig.4-Fig.5). Physically, this indicates the movement of the vortex along the cylinder surface.

When discussing the principal component, the contribution rate reflects energy percentage of one principal component in all components. The contribution rate of *i*th principal component can be defined as

$$CR_i = \frac{\lambda_i}{\sum_1^n \lambda_i} \tag{8}$$

Where λ_i is the value of the *i*th eigenvalue mentioned in section 2.2 and $\sum_1^n \lambda_i$ is the sum of all the eigenvalues.

Fig.6 depicts the contribution rate of the first fifteen eigenvalues. The first and second principal components of the pressure changes account for more than 99.8% of the total changes on the cylinder surface, which suggests that the first and second principal components of the pressure distribution around the cylinder account for most of the total variance of the pressure field without losing much information.

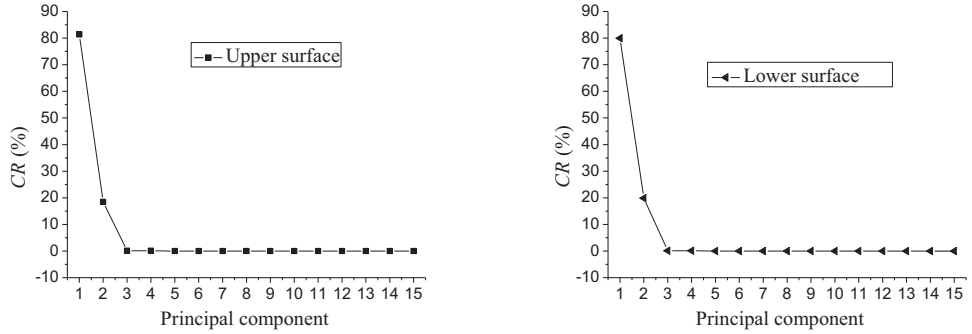

Fig.6. Contribution rate of the principal component on upper and lower surface.

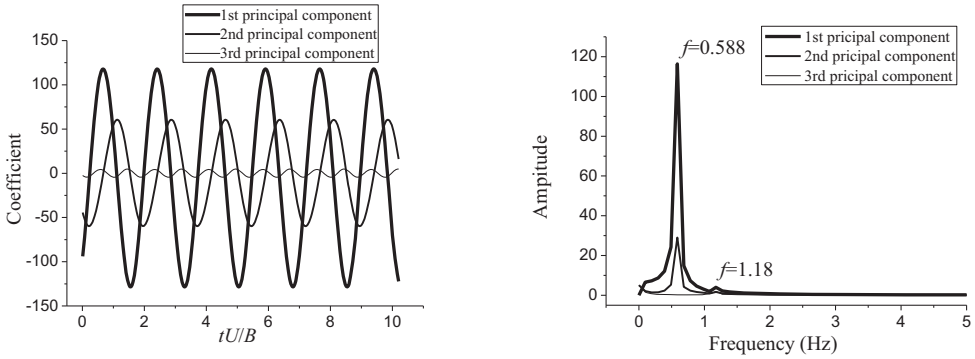

Fig.7. Coefficients and FFT analysis of first 3 principal components on upper surface.

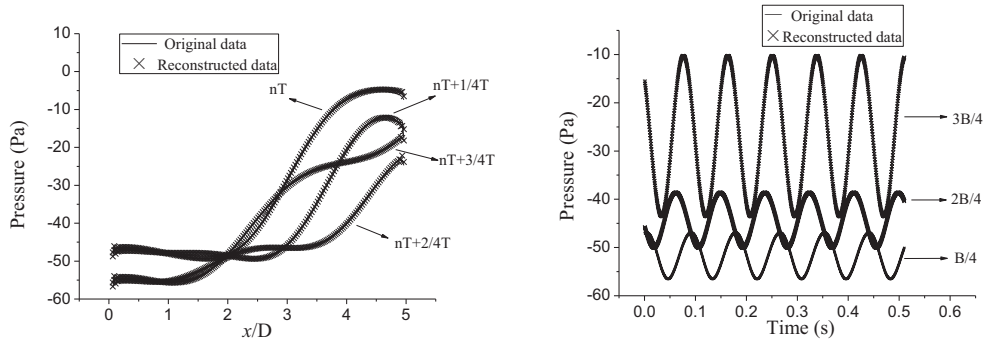

Fig.8. Reconstruction of fluctuating pressure on upper surface (B is width of cylinder).

As mentioned in section 2.2, the coefficients fluctuation of the principal component can be calculated, as shown in Fig.7. From the FFT analysis of the coefficients, one can find that a dominant frequency has been observed from both of the coefficients, with the first and second principal components showing the same frequency. Comparison shows that this frequency agrees well with the Strouhal number. Thus, the frequency feature of the coefficients can be related to the vortex shedding of the flow. A small peak also appears on the spectrum of the third principal component (right in Fig.7). Physically, this is related to smaller eddies and scales in the flow accompanying the main vortex mentioned above. Fig.7 also verifies that the first and second principal component contain most of the variable information, corresponding to the main vortex shedding.

Now that the first two principal components are responsible for the main fluctuation of pressure fluctuation along the surfaces, then we can reconstruct the time-dependent pressure on the surface of cylinder based on the Eq.6. Fig.8 shows the original and reconstructed transient pressure data (left) and time history of pressure at prescribed positions (right) on upper surface. Obviously, the reconstructed data agrees well with the computed data which indicates that the first principal component is enough to reconstruct the fluctuating pressure data along the surface. From Fig.8 (right) we can find that maximum pressure fluctuation occurs at x/D=3B/4, which can also be seen from RMS values of pressure in Fig.2.

From all mentioned above, PCA is proved to be useful and efficient for dealing with the nature of pressure distribution along the surface and original data can be easily reconstructed with few principal components without losing much information.

4.3 Effects of Reynolds number

In this section, effects of Reynolds number on flow characteristics are simulated and discussed. Table.3 lists the several cases performed in this paper, Reynolds number ranges from 1.03×10^4 to 1.03×10^6.

Fig.9 shows the Strouhal number and drag coefficient is insensitive to the variation of the Reynolds number in the range investigated, which has been verified in wind tunnel test. The tendency of 2-D $SST\ \ k-\omega$ model to underestimate the base pressure may be responsible for the overestimation of drag coefficient. From Table.3 one can find the standard deviation of lift and drag coefficient $C_L^{'}$ and $C_D^{'}$ decrease intensely with the increase of Reynolds number.

Table.3. Effects of Re number on aerodynamic parameters

Case	Reynolds number	Velocity (m/s)	max y^+	Time step	St	C_D	$C_L^{'}$	$C_D^{'}$
1	1.03×10^4	0.3	6.0E-03	0.010	0.117	1.14	0.22	0.035
2	3.42×10^4	1.0	1.5E-02	0.001	0.120	1.14	0.20	0.022
3	5.13×10^4	1.5	2.0E-02	0.002	0.119	1.13	0.19	0.017
4	1.03×10^5	3.0	3.5E-02	0.0015	0.113	1.11	0.18	0.013
5	3.42×10^5	10	0.8E-01	0.0005	0.113	1.09	0.16	0.009
6	6.84×10^5	20	1.5E-01	0.0002	0.112	1.10	0.15	0.008
7	1.03×10^6	30	2.3E-01	0.0001	0.113	1.11	0.16	0.009

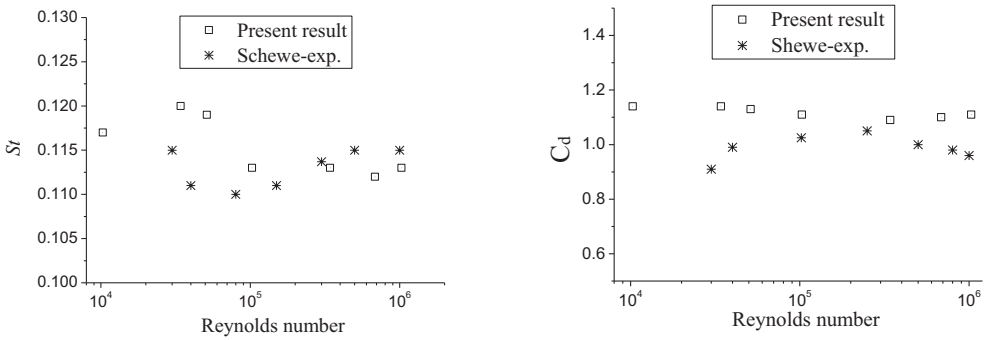

Fig.9. Strouhal number and drag coefficient as function of varying Reynolds number: comparison of current numerical results and experimental result from Schewe (2009).

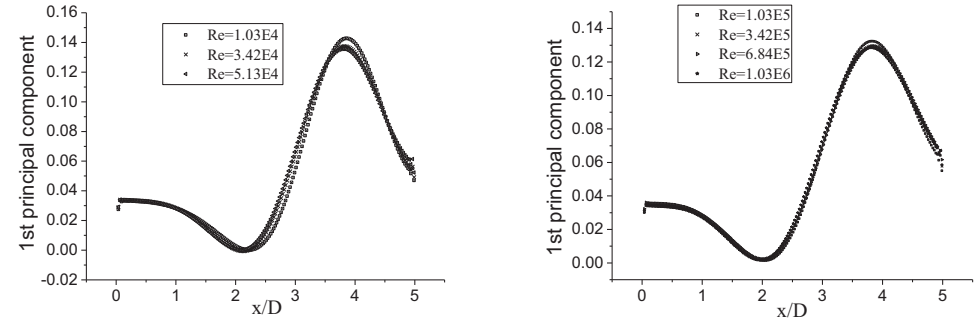

Fig.10. First principal component on the upper surface as functions of varying Reynolds number.

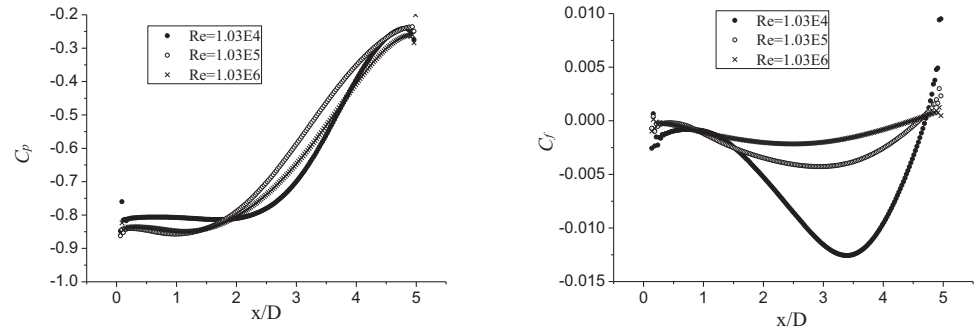

Fig.11. The mean pressure and friction coefficient on the upper surface as functions of varying Reynolds number.

The distribution of the first principal component on upper surface with the varying Reynolds number is depicted in Fig.10. It is found that similar mode is found when the Reynolds number exceeds 1.03×10^5, while less than it the peak of the first principal component will close to the trailing edge as the Reynolds number decreases. Fig.18 displays the mean pressure and friction coefficient on the upper surface as functions of Reynolds number. Similarly, mean pressure coefficient exhibit the same tendency at Re number larger than 1.03×10^5, while Re number is under 1.03×10^4 the position of pressure recovery lag behind the location in case of Re number larger than 1.03×10^5 on the upper surface. This phenomenon can be analyzed from the position of bubble vortices on the surface as shown in Fig.11 (right). The local valley in mean friction coefficient distribution is considered to be the position of the centre of the time-averaged bubble vortices. It is clear that when Re is smaller than 1.03×10^5 the position is closer to trailing edge which impedes the flow reattachment on former portion.

5 CONCLUSIONS

This paper provides the fundamental flow characteristics around the 1:5 rectangle cylinder, and compares the resuts with the experiments.

Main conclusions are included as following:

(1) Consequently, good agreement with the experiment is obtained. According to the numerical result of *St* and force coefficient, 2-D numerical simulation is proved efficient and reliable, which indicates that 2-D numerical simulation can satisfy the engineering requirement.

(2) Based on the distribution of the RMS values of pressure fluctuation, mean vortex shedding position is considered at x/D=3.85 and the fluctuating pressure distribution is considered to 3-D effects. Moreover the numerical flow visualization is provided to better understand the change of aerodynamic force on the side surface of the rectangular cylinder.

(3) Based on the PCA method, the nature of the pressure fluctuation is analyzed in this paper. It is found that the first two principal components are enough to contain the pressure fluctuation information. Furthermore, the pressure is reconstructed with few principal components, verifying the reliability of PCA and providing a feasible method to save the countless data extracted from experiment or numerical simulation. Analysis from the PCA also indicates that the first two modes are mainly responsible for the variations of the pressure on the side surface of this bluff body.

(4) At last, effects of Reynolds number on those flow characteristics are discussed. Changes of *St*, C_D, C_L', C_D', C_P, C_f and principal components varying as the function of Reynolds number are included. Generally, the *St* and C_D are insensitive to the changes of Reynolds number in present Re number range research while C_L' and C_D' both exhibit intensive decline as the Reynolds number increases. As for the C_P, C_f and the principal components, Re=1.03×10^5 is considered to be a critical values for the remarkable changes of those flow characteristics.

Further studies are required to explore the nature of the pressure distribution on the surface of the bluff body based on 3-D numerical simulation and to confirm the present assertion about the effects of Re number on C_P, C_f.

REFERENCES

D. K. Tafti and S. P. Vanka. A numerical study of flow separation and reattachment on a blunt plate. Phys. Fluids July 1991A 3(7) 1749-1759.

Caludio Mannini, Numerical investigation on the three-dimensional unsteady flow past a 5:1 rectangular cylinder, J. Wind Eng. Ind. Aerodyn.99(2011)469-482.

Claudio Mannini,Unsteady RANS modeling of flow past a rectangular cylinder: Investigation of Reynolds number effects, Computers & Fluid 39(2010) 1609-1624

Luca Bruno, 3D flow around a rectangular cylinder: A computational study, J. Wind Eng. Ind. Aerodyn. 98(2010) 263-276

Holmes J D, Analysis and synthesis of pressure fluctuations on bluff bodies using eigenvetors, Journal of Wind Engineering and Industrial Aerodynamics, 1990, Vol.33, p. 219-230.

Schewe G. Reynolds-numer-effects in flow around a rectangular cylinder with aspect ratio 1:5. In: Borri C, Augusti G, Bartoli G, Facchini L, editors. Proc 5th European and African conference on wind engineering, Florence, Italy. Florence: Firenze University Press; 2009

Matsumoto, M., Shirato,H., Aaraki, k., Haramura,T., Hashimoto, T. Spanwise coherence characteristic of surface pressure field on 2D bluff bodies. Journal of Wind Engineering and Industrial Aerodynamics 2002 91, 155-163

Shimada K, Ishihara T. Application of a k-ε model to the prediction of aerodynamic characteristics of rectangular cross-section cylinders. J fluids Struct 2002; 16(4): 465-85.

D. Yu, A. Kareem. Two=dimensional simulation of flow around rectangular prisms. Journal of Wind Engineering and Industrial Aerodynamics 62 (1996) 131-161.